Equilateral Triangular Dielectric Resonator and Metal Patch Hybrid Antenna for UWB Application

ZHIWEI SONG[1], **HONGXING ZHENG**[2], **(Member, IEEE), MENGJUN WANG**[2], **YAN LI**[3], **TAO SONG**[2], **ERPING LI**[4], **(Fellow, IEEE), AND YONGJIAN LI**[1], **(Member, IEEE)**

[1]State Key Laboratory of Reliability and Intelligence of Electrical Equipment, Hebei University of Technology, Tianjin 300130, China
[2]School of Electronics and Information Engineering, Hebei University of Technology, Tianjin 300130, China
[3]College of Information Engineering, China Jiliang University, Hangzhou 310018, China
[4]Zhejiang University-UIUC Institute, Zhejiang University, Hangzhou 310027, China

Corresponding author: Hongxing Zheng (hxzheng@hebut.edu.cn)

ABSTRACT This paper postulates a novel omnidirectional low-profile ultra-wideband (UWB) antenna, which is structured by discrete embedded dielectric resonator antenna with features of both low-profile dielectric resonator (DR) and thin planar monopole antenna, where the laminated equilateral triangular DR and the rectangular metal patch monopole are stacked up. This new design can lower the profile of the antenna. Furthermore, the symmetric DR and the monopole structure are able to make the surface currents in some operating modes opposite in phase, together with the characteristics of the coplanar waveguide (CPW) feed structure and the DR, the cross-polarization is reduced effectively. The mode analysis has been done to show how the antenna achieves the UWB. The CPW which can integrate with integrated circuits easily is used to provide the excitation source. The antenna provides consistent omnidirectivity, consistent gain, low cross-polarization, and high-radiation efficiency within the entire operation band. A prototype (dimensions are 17.6 mm × 33.6 mm and 1.524 mm thickness) is fabricated and measured. The measurements are well correlated with the simulations.

INDEX TERMS Defected ground structure, dielectric resonator, discrete embedded, hybrid antenna, low-profile, low cross-polarization, omnidirectional, ultra-wideband.

I. INTRODUCTION

It is well-known that the ultra-wide-band (UWB) system has many attractive advantages and antenna plays a very important role in the system. The UWB antenna has an extremely wide operation bandwidth within the microwave range, and a very low emission limit. Since the UWB antenna has so many merits, lots of researchers have worked in this field [1]–[5]. Whereas, there are some major challenges for the design of UWB antennas including: achieve sufficient impedance matching bandwidth, the interference problem is caused by the nearby wireless communication band, compact antenna size, high radiation efficiency, and how to get a consistent uniform radiation pattern to avoid undesirable distortions of the radiated and received pulse [6]. Most of the recent works aim at improving the performance of the UWB antenna, especially to avoid the interference problem [7]–[11].

Nevertheless, the radiation patterns are still problematic because the omnidirectivity usually cannot be realized in high frequency band (see [11] for detail information). There are many literatures on methods to improve the omnidirectivity of radiation pattern in the entire operation frequency band. Those methods include use a combination mechanism of the inserted structure [12], modify the antenna ground plane shape [13], determine the dominant mode at high and low frequencies [14], and use an ordinary square radiating patch [15]. As is well known, planar broadband monopole antennas suffer high cross-polarization [6]. Whereas, only a few reported studies have worked on reducing the cross-polarization but keeping the consistent omnidirectional patterns for the planar monopole antennas. What's more, when planar monopole antennas work in the high frequency band, their surface wave loss and conduct loss are much higher.

On the other hand, the dielectric resonator antenna (DRA) is one of the better alternatives for UWB application due to

The associate editor coordinating the review of this article and approving it for publication was Lu Guo.

several merits such as high radiation efficiency, low surface wave loss, negligible conductor loss, light weight, small size, and robustness to machining tolerance. Whereas, the DRA has high Q-factor usually suffers a narrow band characteristic, and the profile of the DRA is relatively high in the reported works. So as to alleviate this problem, many studies on DRA bandwidth enhancement have been reported in the past two decades [16]–[28]. In order to expand the DRA bandwidth, So and Leung groove a rectangular slot in the ground plane [16]. Chair, Kishk, and Lee excite the dominant mode and high order modes to enhance the DRA bandwidth [17]. The enhancement is realized by inserting a stub into the center of a U-shaped feedline in [18]. Multilayered structure (each layer with a different permittivity) is used to enhance the bandwidth in [20]–[22]. Monopole and different hybrid dielectric resonator structures are used to expand the DRA bandwidth in [23]–[26].

Nowadays, various types of portable wireless communication devices are around us, and these devices usually with small sizes, so antennas of low-profile design are desired. Take the smart mobile phone as an example, its profile is usually around 7 mm. The screen, integrated circuit, and protective containment takes 3 mm - 5 mm, thus the space for antennas to be integrated in is narrow. So the miniaturized and low profile antennas are desired design. Meanwhile, most of the reported DRAs are of high thickness. Some works have been done to lower the profile of the DRA, but their profiles are still more than 5 mm [20], [24], and [29].

In this paper, a coupled DR and metal patch antenna is postulated. The combination mechanism of quasi-square planar monopole (inserted structure) and laminated DRs fed by the co-planar waveguide (CPW) can provide an excellent consistent omnidirectional radiation pattern and achieve low cross-polarization in the entire operating frequency band. The discrete embedded method is used to lower the antenna profile and the entire profile has been reduced to 1.524 mm. What's more, the bottom plane of the antenna is a monolithic flat surface, so the antenna can be combined with integrated circuits easily.

This paper is organized as follows. The geometry of the proposed antenna is introduced in Section II. The antenna design and working mode analysis are presented in section III. The simulated radiation characteristics are given in Section IV. Section V illustrates the simulated and measured results. Section VI summarizes the antenna design process. The conclusion is drawn in the last section.

II. ANTENNA CONFIGURATION

The geometry of the proposed DR and metal patch hybrid antenna is shown in Fig. 1. Each laminated equilateral triangular DR ($\varepsilon_r = 20.0$, $\tan\delta = 0.002$) has 16.4 mm length of side. The rectangular dielectric substrate ($\varepsilon_r = 3.0$, $\tan\delta = 0.0013$) size is 17.6 mm × 33.6 mm. And all the DRs and dielectric substrate have a thickness of 0.762 mm. An equilateral triangle which slightly larger than the DR is engraved in the dielectric substrate to let one DR be embed in, then
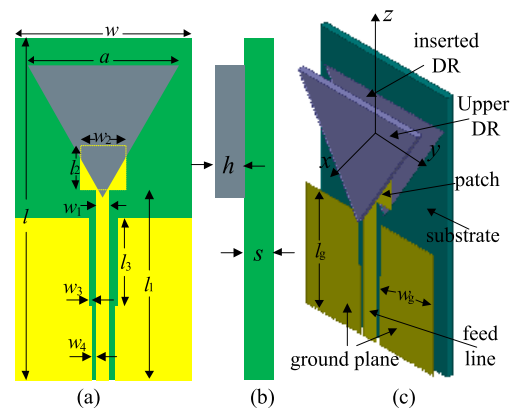

FIGURE 1. Geometry of the proposed ultra-wide-band omnidirectional low-profile discrete embedded antenna. (a) Front view, (b) Side view, and (c) Exploded pictorial drawing.
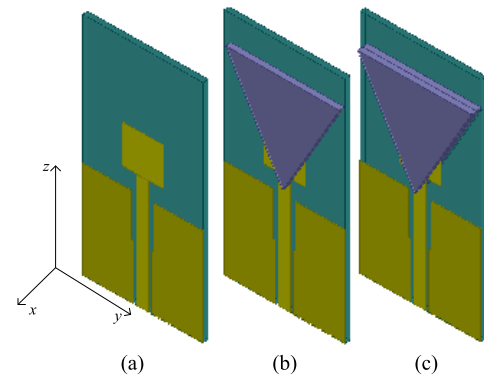

FIGURE 2. Evolution of the proposed antenna: (a) rectangular monopole without DR, (b) rectangular monopole with 1 DR, and (c) the proposed antenna.

TABLE 1. Size of the proposed antenna.

Symbol	Size(mm)	Symbol	Size(mm)
s	0.762	w_2	6.0
h	0.762	l_2	5.7
w	17.6	w_g	7.5
l	33.6	l_g	14.5
a	16.4	w_3	0.4
w_1	1.80	l_3	6.3
l_1	17.0	w_4	0.3
ε_{r1}	3.0	$\mathrm{Tan}\delta_1$	0.0013
ε_{r2}	20.0	$\mathrm{Tan}\delta_2$	0.002

the rectangular planar monopole and CPW feed structure are installed, at last another DR is stacked on top of the embedded one, as shown in Fig.1 (c). The symbols of each parameters of the antenna are shown in Fig. 1. Evolution of the proposed antenna is shown in Fig. 2. All of the three antennas have been simulated in the high frequency structure simulator (HFSS). Many of the parameters can affect the antenna performances significantly. We use the parameter sweeping function of HFSS to find the final sizes which are tabulated in Table 1.
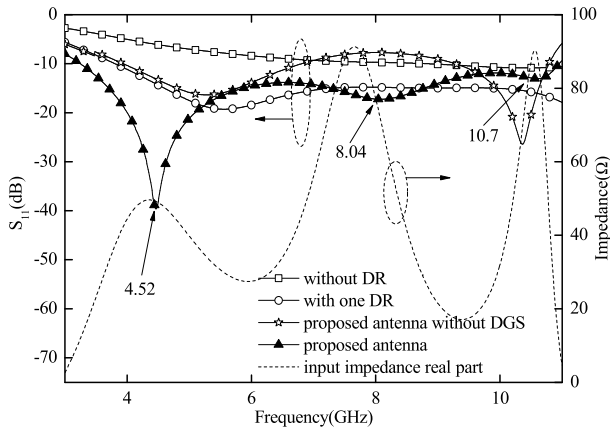
FIGURE 3. The simulated S$_{11}$ of four antennas with different geometry, and impedance real part of the proposed antenna use the parameters in table 1.

The simulated S$_{11}$ of some antennas with the above mentioned parameters but different configurations are shown in Fig. 3. It is clear that the S$_{11}$ is great than -10 dB when the antenna with the structure shown in Fig. 2(a). As for the antenna with the structure shown in Fig. 2(b), the operating frequency is reduced significantly and the S$_{11}$ is better because material with high permittivity is inserted. When the antenna with the proposed structure but without the defected ground structure (DGS) (line with stars), there are only two working frequencies at 5.1 GHz and 10.1 GHz, respectively. When the antenna has the proposed structure as shown in Fig. 2(c) i.e. etched DGS in the ground plane, the operating frequency band is wider (the middle frequency is gained) and the impedance matching is obviously improved. The proposed antenna has three working frequencies at 4.52 GHz, 8.04 GHz and 10.7 GHz, covers 3.2 GHz to 10.96 GHz in the simulation. It is clear that the hybrid antenna can match the UWB design goal very well from the simulated S$_{11}$.

## III. MODE ANALYSES, ANTENNA DESIGN, AND NUMERICAL INVESTIGATION

For the sake of achieve UWB characteristic, different working modes of the hybrid antenna have been excited. The monomeric equilateral triangular DR mode analysis can be found in [30] and [31]. However, all of the analyses are about antennas which are working under TM modes. In our design, the antenna is omnidirectivity, so the DRs in this antenna are working under TE modes. Furthermore, when the antenna has the geometry as shown in Fig. 1, it operates under TE$^x_{\delta mn}$ modes. In order to carry out the analysis of the DRs under TE modes, we can refer to the analyses of metal waveguide with perfect conductor boundary under TM modes [32]. The cut-off frequency in TE modes of DR can be calculated as follows, we have

$$\chi = \frac{4\pi}{3a}\sqrt{\left(m^2 + mn + n^2\right)} \qquad (1)$$

$$f_c = \frac{\chi v}{2\pi} == \frac{2c\sqrt{\left(m^2 + mn + n^2\right)}}{3a\sqrt{\varepsilon_r}} \qquad (2)$$

where f_c is the cut-off frequency, c is the light speed in free space, m and n are integers, a is the length of side of the equilateral triangular DR, and ε_r is the relative permittivity of the DR.

The antenna is designed to cover 3.1 GHz - 10.6 GHz, therefore we roughly choose the fundamental mode (TE$^x_{\delta 11}$) working at 5.0 GHz, because the permittivity of the DR we choose is 20.0, after use (2), we have $a \approx 15.49$mm. In this condition, the antenna has two operating frequencies at 4.85 GHz and 10.88 GHz correspond to fundamental mode and high order mode, respectively. We insert monopole into the DRs and design the monopole operating at around 7.0 GHz, so the width (w_2) of the monopole is about 6.18 mm ($\lambda/4$), when $w_2 = 6$ mm, the antenna operating at 6.8 GHz as shown in Fig. 4 (green solid line). But the impedance matching of the antenna is not good enough, so the DGS is etched in the ground plane. At last, the parameter scanning function of HFSS is used to find the final sizes of the proposed antenna.
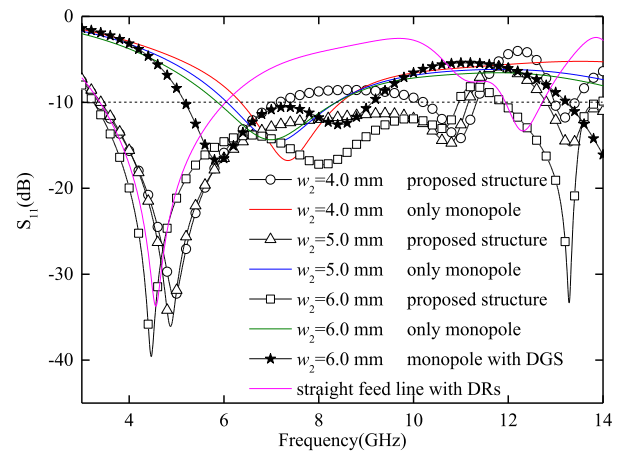
FIGURE 4. The simulated S$_{11}$ when the antenna with different geometries and different rectangular monopole width (w_2).

The simulated S$_{11}$ are shown in Fig. 4 when the antenna has different geometries and different rectangular monopole widths (w_2). The violet line corresponds to the simulated S$_{11}$ when the DRA is excited by straight feedline. It is clear that the DRA has two operating frequencies at 4.56 GHz and 12.31 GHz. Meanwhile, the calculated cut-off frequencies are 4.72 GHz (correspond with TE$^x_{\delta 11}$ mode) and 12.19 GHz (correspond with TE$^x_{\delta 14}$ mode). The calculated results are reasonably agreement with the simulated ones. The proposed antenna has three operating frequencies (the line with hollow squares). The middle operating frequency is mainly caused by rectangular monopole and the DGS [12]. From Fig. 4 we can see the operating frequencies changes to around 7.4 GHz when the rectangular patch has different width (the red, blue and green lines). When antenna is the combine of the patch and DGS only, the operation band can cover 5.18 GHz to
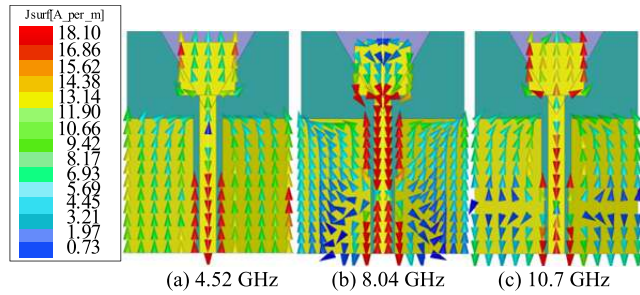
FIGURE 5. The surface current distribution on the rectangular monopole and the ground plane at different operating frequencies in 'yoz' plane (x = 0), (a) 4.52 GHz, (b) 8.04 GHz, (c) 10.7 GHz (from HFSS).

FIGURE 6. The three-dimensional field distribution, (a) and (b) for E- and (c) and (d) for H- when the DRs operating at difference frequencies (from HFSS).

FIGURE 7. The simulated S_{11} of the antenna when the DR with different parameters. h = 0.762, 1.0, and 1.25 mm, a = 15.6, 16.4, and 17.3 mm, ε_r = 10.0, 20.0, and 30.0.

9.12 GHz. In addition, the simulated S_{11} which are shown by three lines with symbols correspond to the antenna with the proposed structure but with different patch width. When the patch width is changed, the S_{11} at the upper and lower operating frequencies changes a little, whereas the S_{11} changes a lot at the middle operating frequency. This proves that the middle operating frequency is mainly caused by the patch and DGS. The couplings among antenna components make it operating at 4.52 GHz, 8.04 GHz and 10.7 GHz in simulation. The simulated current distributions of patch and DGS at 4.52 GHz, 8.04 GHz and 10.7 GHz are shown in Fig. 5. Their current intensity of the monopole and the DGS is the strongest at 8.04 GHz. That means the monopole and the DGS play a very important role in radiation at this frequency.

Next, we do the further modes analyses considering HFSS simulation results. To validate the results of the analyses, the simulated S_{11} of different antennas are shown in Fig. 3. The minima of S_{11} may not correspond with the actual working frequency of the antenna exactly. So, in order to predict the correct number of working modes, the real part of the input impedance is utilized, and the simulated result is shown in Fig. 3 too. The simulated results agree with the analyses reasonably. In order to verify the DR operating modes, the distributions of three-dimensional E- and H-fields are shown in Fig. 6 at 4.52 GHz and 10.7 GHz. We can see that the H- fields have components in all three coordinate axes. Whereas the E-fields have components in y-axis and z-axis only out of therectangular metal patch area. Since E-field perpendicular to the metal patch, there are E_x components in the metal patch area. So, if only the DR, it is operating under $TE^x_{\delta mn}$ modes. The 4.52 GHz associates with $TE^x_{\delta 11}$ mode and the10.7 GHz associates with $TE^x_{\delta 14}$ mode therein.

Useful numerical investigations will be given in order to provide mode analyses with powerful support. The simulated S_{11} of the equilateral triangular DR with different parameters is shown in Fig. 7. Note: h = 0.762 mm, a = 16.4 mm, and ε_r = 20.0 correspond to the proposed antenna, so the simulation results are overlapped. It is clear that as the thickness and length of side of the DR change, the upper and lower operating frequencies change faster than the middle one. Means that the upper and lower operating frequencies are mainly excited by the DRs. The dielectric constant of the equilateral
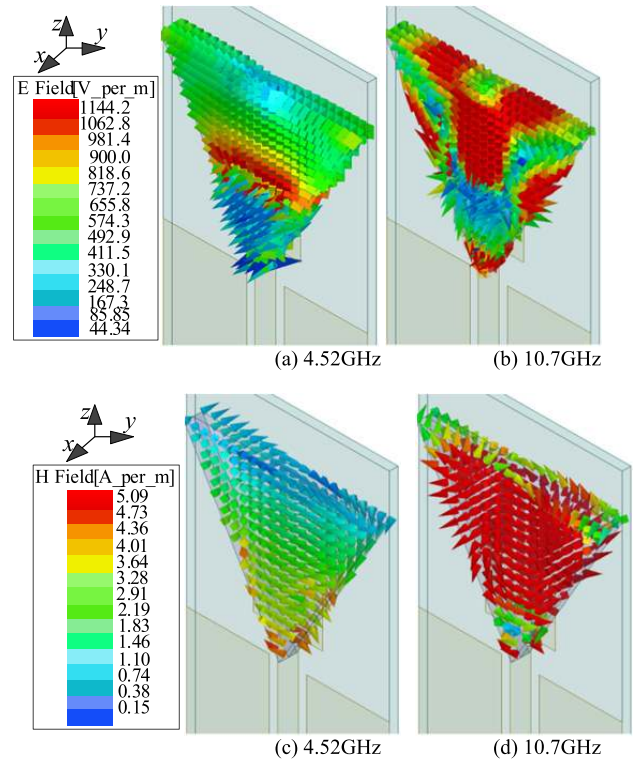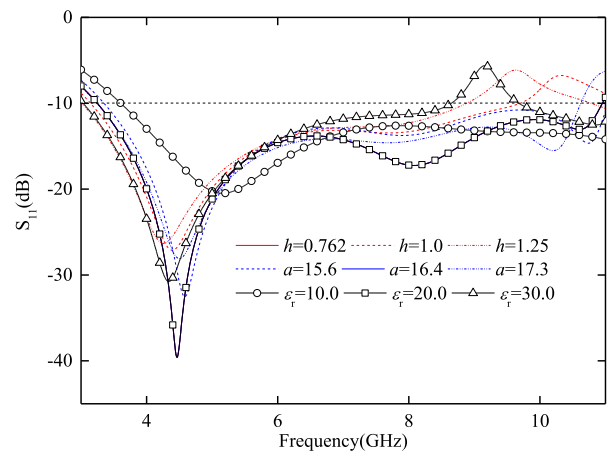
triangular DR affects S_{11} greatly and the simulations are shown in Fig.7, too. When the dielectric constant increases the operating frequencies decrease, the operation bandwidth decreases, and the impedance matching change greatly. And all the operating frequencies have a large variation, since operating frequency is inversely proportional to effective permittivity in the approximate calculation formula. Meanwhile one DR is embedded in the substrate and as a part of it, so the substrate relative permittivity is also changed. The DGS or
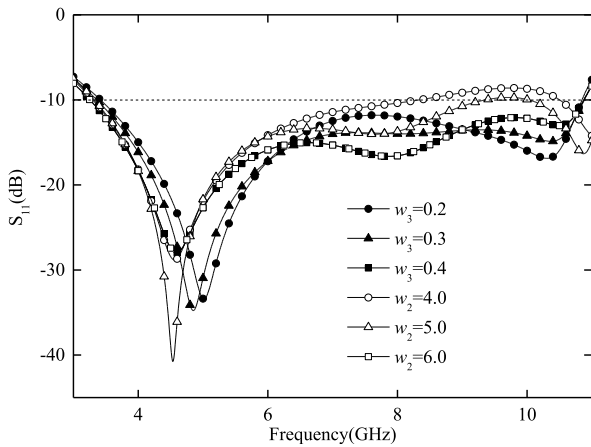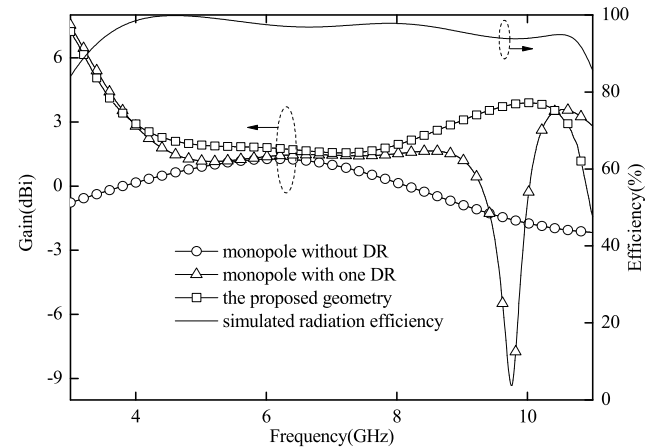
FIGURE 8. The simulated S$_{11}$ of the antenna when defected ground plane and monopole in different widths. w_3 = 0.2, 0.3, and 0.4 mm and w_2 = 4.0, 5.0, and 6.0 mm. The two lines with squares are overlapped due to them with same parameters sizes.

FIGURE 10. The simulated gain of three different antennas with the same parameters sizes in table 1, and the simulated radiation efficiency of the proposed antenna.

monopole widths can affect S$_{11}$ greatly too, and the simulated S$_{11}$ are shown in Fig. 8. Obviously, when the DGS width changes, the upper operating frequency keeps nearly constant, but the lower two change greatly; when the monopole width changes, the lower operating frequency keeps nearly constant, but the upper two change greatly. We can conclude that the change in DGS and monopole width can affect the operating frequency of the antenna. Especially, their width determines the middle working frequency.

IV. RADIATION CHARACTERISTIC

The simulated cross- and co-polarization of the E- and H-fields at different working frequencies of the proposed antenna are shown in Fig. 9. Seen from Fig. 9 (a), the cross-polarization of the E-fields at two low working frequencies are at least 35 dB lower than co-polarization in most directions. And the radiation pattern changes a little in the entire working frequency band. The deviations between the cross- and co-polarization of H-fields are more than 21 dB in most directions at 4.52 GHz and 8.04 GHz, and the deviation is still more than 16 dB in most directions at 10.7 GHz as shown

FIGURE 9. The simulated E- and H-plane radiation patterns of the antenna at different operating frequencies with the parameters in table 1. Red solid line 4.52GHz, blue dash line 8.04 GHz, violet dash-dot-dot line 10.7 GHz.
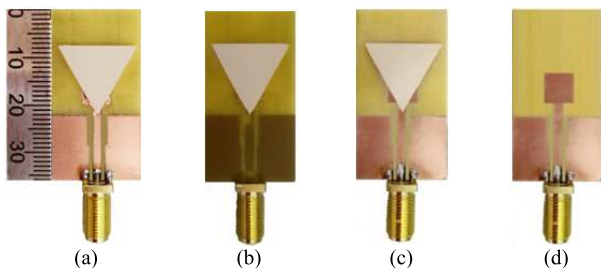
in Fig. 9 (b). That is because the surface currents in some operating modes are opposite in phase. Therefore, some surface currents cancel each other, which is beneficial to reduce the cross-polarization of the antenna. In addition, the CPW feed structure and DRs are also contributed to reduce the cross-polarization. Unlike microstrip line feed structure the CPW has less effect in the fringing fields between feedline and the ground plane, so the cross-polarization which is caused by the microstrip line discontinuity is removed. And the polarization currents which are induced in the DRs has no sharp edge current component rather than the conduction currents which are induced on the planar printed UWB antennas which concentrate at the edges that contribute to the high cross-polarization. The radiation pattern of H-fields at each working frequency point is omnidirectivity, and the co-polarization radiation patterns on the H-plane keep constant. After the analysis of the antenna far fields radiation patterns, the gain comparison of three antennas in different geometry but with the same sizes are shown in Fig. 10. The gain of the antenna when the rectangular planar monopole as its only radiator is represented by the hollow circles line and is the lowest of the three curves. And the gain is minus in most of the working frequency band. When the rectangular planar monopole and one DR are applied as the radiator, its gain is higher than the one mentioned above, but the gain is not stable enough in the working frequency band, especially in the 9 GHz - 10.4 GHz, and the lowest gain is around −9 dBi at 9.78 GHz. The gain of the antenna is improved by the proposed structure, and in more than half of the working frequency band the gain is greater than 2.0 dBi. The proposed antenna is omnidirectional, and its gain is higher than the traditional microstrip antenna, so the radiation efficiency is also higher. In order to prove the above analysis results, the simulated radiation efficiency of the proposed antenna is shown in Fig. 10 (solid line). It is clear that the radiation efficiency is greater than 95.6% in the whole working frequency band.
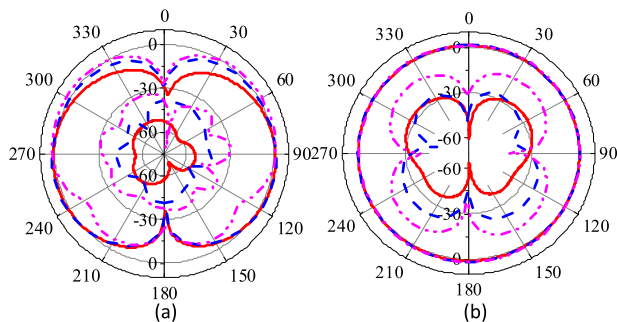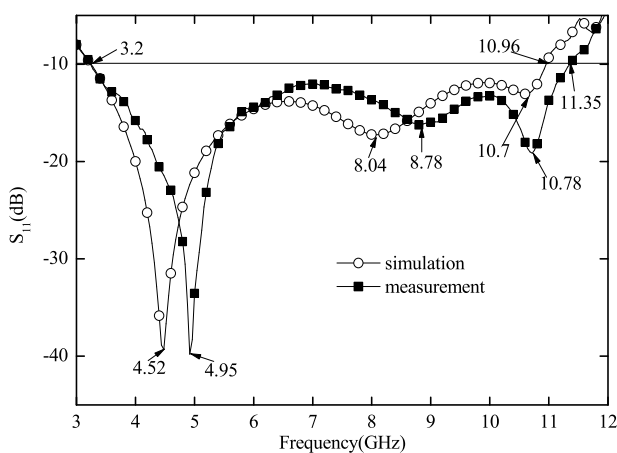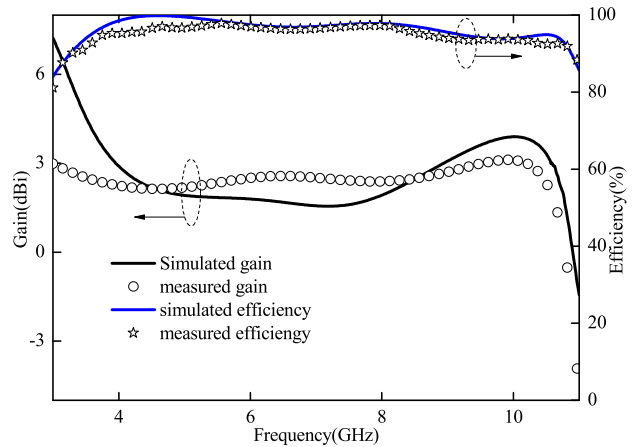
V. RESULTS AND DISCUSSION

The three fabricated samples are shown in Fig. 11. All of them have been measured, but here only the measurements of the proposed antenna are shown for brevity. The measurements are performed by using the Agilent PNA-X network analyzer (N5244A) and the anechoic chamber (OBT6). The simulated and measured S_{11} of the proposed antenna are shown in Fig. 12. The working bandwidth in simulation is from 3.2 GHz to 10.96 GHz (impedance bandwidth, 109.6 %), and from 3.2 GHz to 11.35 GHz (impedance bandwidth, 112 %) in the measurement. The simulation results are in good agreement with the experimental results in most of the working frequency band. The gain and radiation efficiency has been measured, and the results are shown in Fig. 13. The measurements and simulations are also in good agreement. It is clear that the radiation efficiency is greater than 93% in the entire working frequency band. Note: there are derivations between simulations and measurements both in Fig. 12 and Fig. 13. Generally, the radio-frequency cable from the Vector Network Analyzer to the antenna significantly affects the measurements when the tested antenna is installed on a small ground [34]. In addition, the inevitable manufacturing errors and undesirable measuring environment also contributes to measurement error. The radiation patterns of the prototype

FIGURE 13. Comparison results of simulated and measured gain and radiation efficiency. The simulations are represented by the solid lines, and the measurements are represented by the symbols, respectively.

are measured in the anechoic chamber, the simulation results and experimental results are shown in Fig. 14. Obviously the measurement results show that the proposed antenna has low cross-polarization in E-fields and constant omnidirectivity in H-fields in the entire working frequency band. And the measured radiation patterns agree very well with the simulated ones.

A comparison of the proposed antenna with those reported in literature is tabulated in table 2. From the comparison results we can see that the profile of the antenna in our design is the smallest. In addition, the operation bandwidth in our design can cover the FCC ordered UWB frequency band very well. And it is one of the best designs among the mentioned references.

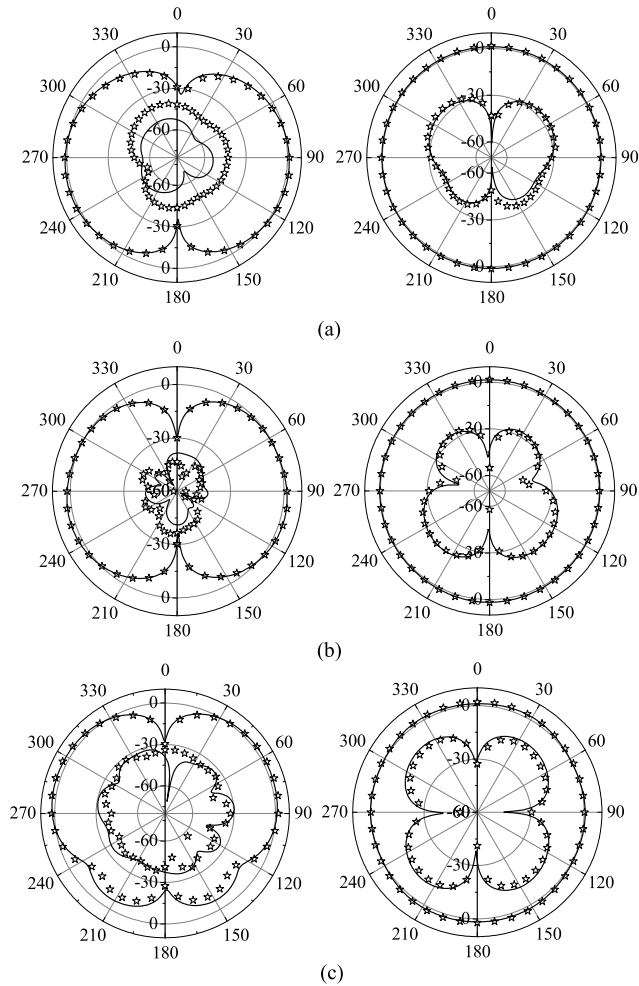**TABLE 2.** Comparison of proposed antenna and reported.

ε_r	Profile	Bandwidth (GHz)	Peek gain (dBi)	Efficiency (%)	Reference
10.0	$0.097\lambda_0$ [a]	6.6-18.5	N/A	N/A	[1]
10.2	$0.055\lambda_0$	3.2-10.8	3.8	>96.5	[12]
10.2	$0.193\lambda_0$	6.9-12.3	N/A	N/A	[20]
10.0	$0.083\lambda_0$	5.0-21.0	4.0	N/A	[22]
10.2	$0.050\lambda_0$	2.9-11.3	6.7	98.3	[28]
20.0	$0.032\lambda_0$	4.8-12.3	3.52	>88	[33]
9.2	$0.155\lambda_0$	3.1-11.6	N/A	N/A	[35]
20.5	$0.231\lambda_0$	10.1-13.0	15.1	N/A	[36]
20.0	$0.012\lambda_0$	3.2-11.35	3.3	>93	Proposed

[a]The symbol λ_0 is the wavelength in free space respect to the lowest operating frequency point.

FIGURE 11. The three fabricated prototypes. The proposed antenna top view and bottom view are shown in (a) and (b), respectively. The third one (c) is of the antenna with 1 DR. The forth one (d) is the rectangular planar monopole antenna.

VI. DISCUSSION

The antenna design process is summarized as follows:

First, we choose equilateral triangular DR as radiator, because compare with rectangular and cylindrical DR the equilateral triangular DR has the smallest volume when they are working at the same frequency. The length of side of the equilateral DR can be calculated by using (2) when the dielectric material and working frequency is chose.

FIGURE 12. Comparison results of simulated and measured S_{11}. The simulation is represented by the line with hollow circles, and the measurement is represented by the line with black blocks, respectively.

FIGURE 14. The measured and simulated radiation patterns in E-fields and H-fields of the proposed antenna at 4.52 GHz, 8.04 GHz and 10.7 GHz operating frequencies, respectively. The amplitude units for every E-fields and H-fields are in dB. The solid lines correspond to simulation results, and the symbols correspond to measurement results.

Second, the length of side (about $\lambda/4$) of the metal patch can be calculated by using (3), after the substrate material and working frequency is selected:

$$w_2 = \frac{c}{4f_c\sqrt{\varepsilon_r}} \qquad (3)$$

where ε_r is the permittivity of the substrate.

Third, in order to reduce the cross-polarization and improve the impedance matching, the rectangular DGS is etched in the ground plane where the current intensity is high. The length of side of the DGS can be calculated as follows:

$$\varepsilon_{eff} \approx \frac{\varepsilon_r + 1}{2} + \frac{\varepsilon_r - 1}{2\sqrt{1 + \frac{12s}{w_1}}} \qquad (4)$$

$$l_n = l_3 + w_3 \qquad (5)$$

$$f_n \approx \frac{c}{4l_n\sqrt{\varepsilon_{eff}}} \qquad (6)$$

where ε_{eff}, ε_r, s, and w_1 are effective dielectric constant, dielectric constant of the substrate, thickness of the substrate, and the width of the feed line, respectively.

Last, build the simulation model of the antenna in HFSS and use the parameter sweeping function to find the final sizes of the antenna.

VII. CONCLUSION

A low-profile DRA with ultra-wideband characteristic is designed by exciting different working modes of the laminated equilateral triangular DR and square metal patch hybrid structure. The cross-polarization is reduced by using the CPW and DGS. And the stability of the radiation pattern is gain in the whole operating frequency band. The measurements show that the antenna provides good omnidirectivity, wide bandwidth about 112 % covers 3.2 GHz - 11.35 GHz, low cross-polarization, consistent gain, and high-radiation efficiency (over 93 %) within the entire working frequency band. Meanwhile, the maximum thickness of the antenna is reduced to 1.524 mm by using the proposed design method. Therefore, the designed antenna is a good candidate in small wireless communication device.

REFERENCES

[1] M. Lapierre, Y. M. M. Antar, A. Ittipiboon, and A. Petosa, "Ultra wideband monopole/dielectric resonator antenna," *IEEE Microw. Wireless Compon. Lett.*, vol. 15, no. 1, pp. 7–9, Jan. 2005.

[2] K. W. Khoo, Z. C. Chen, A. C. W. Lu, V. Sunappan, and L. L. Wai, "Miniaturized multilayer UWB antennas on LTCC," *IEEE Trans. Antennas Propag.*, vol. 57, no. 12, pp. 3988–3992, Dec. 2017.

[3] D. Guha, B. Gupta, and Y. M. M. Antar, "New pawn-shaped dielectric ring resonator loaded hybrid monopole antenna for improved ultrawide bandwidth," *IEEE Antennas Wireless Propag. Lett.*, vol. 8, pp. 1178–1181, 2009.

[4] J. R. Costa, C. R. Medeiros, and C. A. Femandes, "Performance of a crossed exponentially tapered slot antenna for UWB systems," *IEEE Trans. Antennas Propag.*, vol. 57, no. 5, pp. 1345–1353, May 2009.

[5] Y. Ge, K. P. Esselle, and T. S. Bird, "Compact dielectric resonator antennas with ultrawide 60%-110% bandwidth," *IEEE Trans. Antennas Propag.*, vol. 59, no. 9, pp. 3445–3448, Jul. 2011.

[6] Z. N. Chen, *Antennas for Portable Devices*. New York, NY, USA: Wiley, 2007.

[7] A. D. Eva, M. Fabres, M. Ferrando-Bataller, and V. M. R. Penarrocha, "Modal analysis and design of band-notched UWB planar monopole antennas," *IEEE Trans. Antennas Propag.*, vol. 58, no. 5, pp. 1457–1467, May 2010.

[8] T. Dissanayake and K. P. Esselle, "Prediction of the notch frequency of slot loaded printed UWB antennas," *IEEE Trans. Antennas Propag.*, vol. 55, no. 11, pp. 3320–3325, Nov. 2007.

[9] K. Kikuta and A. Hirose, "Narrowband interference mitigation in UWB systems utilizing frequency dependence of null formation in array antennas," *IEEE Access*, vol. 4, pp. 8715–8720, 2016.

[10] K. Srivastava, A. Kumar, B. K. Kanaujia, S. Dwari, A. K. Verma, K. P. Esselle, and R. Mittra, "Integrated GSM-UWB Fibonacci-type antennas with single, dual, and triple notched bands," *IET Microw., Antennas Propag.*, vol. 12, no. 6, pp. 1004–1012, 2018.

[11] K.-L. Wong, S.-W. Su, and C.-L. Tang, "Broadband omnidirectional metal-plate monopole antenna," *IEEE Trans. Antennas Propag.*, vol. 53, no. 1, pp. 581–583, Jan. 2005.

[12] K. S. Ryu and A. A. Kishk, "UWB dielectric resonator antenna having consistent omnidirectional pattern and low cross-polarization characteristics," *IEEE Trans. Antennas Propag.*, vol. 59, no. 4, pp. 1403–1408, Apr. 2011.

[13] N. Fortino, J. Y. Dauvignac, G. Kossiavas, and R. Staraj, "Design optimization of UWB printed antenna for omnidirectional pulse radiation," *IEEE Trans. Antennas Propag.*, vol. 56, no. 7, pp. 1875–1881, Jul. 2008.

[14] F. Fereidoony, S. Chamaani, and S. A. Mirtaheri, "Systematic design of UWB monopole antennas with stable omnidirectional radiation pattern," *IEEE Antennas Wireless Propag. Lett.*, vol. 11, pp. 752–755, 2012.

[15] N. Ojaroudi, M. Ojaroudi, and N. Ghadimi, "UWB omnidirectional square monopole antenna for use in circular cylindrical microwave imaging systems," *IEEE Antennas Wireless Propag. Lett.*, vol. 11, pp. 1350–1353, Nov. 2012.

[16] K. K. So and K. W. Leung, "Bandwidth enhancement and frequency tuning of the dielectric resonator antenna using a parasitic slot in the ground plane," *IEEE Trans. Antennas Propag.*, vol. 53, no. 12, pp. 4169–4172, Dec. 2005.

[17] R. Chair, A. A. Kishk, and K. F. Lee, "Wideband simple cylindrical dielectric resonator antennas," *IEEE Microw. Wireless Compon. Lett.*, vol. 15, no. 4, pp. 241–243, Apr. 2005.

[18] M. Abedian, S. K. A. Rahim, S. Danesh, S. Hakimi, L. Y. Cheong, and M. H. Jamaluddin, "Novel design of compact UWB dielectric resonator antenna with dual-band-rejection characteristics for WiMAX/WLAN bands," *IEEE Antennas Wireless Propag. Lett.*, vol. 14, pp. 245–248, Feb. 2015.

[19] R. Chair, S. L. S. Yang, A. A. Kishk, K. F. Lee, and K. M. Luk, "Aperture fed wideband circularly polarized rectangular stair shaped dielectric resonator antenna," *IEEE Trans. Antennas Propag.*, vol. 54, no. 4, pp. 1350–1352, Apr. 2006.

[20] W. Huang and A. A. Kishk, "Compact wideband multi-layer cylindrical dielectric resonator antennas," *IET Microw., Antennas Propag.*, vol. 1, no. 5, pp. 998–1005, Oct. 2007.

[21] H. B. B. Rocha, F. N. A. Freire, R. S. T. M. Sohn, M. G. Da Silva, M. R. P. Santos, C. C. M. Junqueira, T. Cordaro, and A. S. B. Sombra, "Bandwidth enhancement of stacked dielectric resonator antennas excited by a coaxial probe: An experimental and numerical investigation," *IET Microw., Antennas Propag.*, vol. 2, no. 6, pp. 580–587, Sep. 2008.

[22] M. Abedian, S. K. A. Rahim, and M. Khalily, "Two-segments compact dielectric resonator antenna for UWB application," *IEEE Antennas Wireless Propag. Lett.*, vol. 11, pp. 1533–1536, 2012.

[23] O. M. H. Ahmed, A. R. Sebak, and T. A. Denidni, "Compact UWB printed monopole loaded with dielectric resonator antenna," *Electron. Lett.*, vol. 47, no. 1, pp. 7–8, Jan. 2011.

[24] D. Guha, B. Gupta, and Y. M. M. Antar, "Hybrid monopole-DRAs using hemispherical/conical-shaped dielectric ring resonators: Improved ultrawideband designs," *IEEE Trans. Antennas Propag.*, vol. 60, no. 1, pp. 393–398, Jan. 2012.

[25] A. Azari, A. Ismail, A. Sali, and F. Hashim, "A new super wideband fractal monopole-dielectric resonator antenna," *IEEE Antennas Wireless Propag. Lett.*, vol. 12, pp. 1014–1016, Aug. 2013.

[26] C. Ozzaim, F. Ustuner, and N. Tarim, "Stacked conical ring dielectric resonator antenna excited by a monopole for improved ultrawide bandwidth," *IEEE Trans. Antennas Propag.*, vol. 61, no. 3, pp. 1435–1438, Mar. 2013.

[27] Y. F. Wang, N. Z. Wang, T. A. Denidni, Q. S. Zeng, and G. Wei, "Integrated ultrawideband/narrowband rectangular dielectric resonator antenna for cognitive radio," *IEEE Antennas Wireless Propag. Lett.*, vol. 13, pp. 694–697, 2014.

[28] I. Messaoudene, T. A. Denidni, and A. Benghalia, "Ultra-wideband DRA integrated with narrow-band slot antenna," *Electron. Lett.*, vol. 50, no. 3, pp. 139–141, Jan. 2014.

[29] X.-Y. Dong, W.-W. Yang, H. Tang, and J.-X. Chen, "Wideband low-profile dielectric resonator antenna with a lattice structure," *Electron. Lett.*, vol. 53, no. 19, pp. 1289–1290, Sep. 2017.

[30] H. Y. Lo, K. W. Leung, K. M. Luk, and E. K. N. Yung, "Low profile equilateral-triangular dielectric resonator antenna of very high permittivity," *Electron. Lett.*, vol. 35, no. 25, pp. 2164–2166, Dec. 1999.

[31] R. Sengupta, S. Ghosh, S. N. Ray, S. K. Das, M. Gangopadhyay, S. Maity, and B. Gill, "On the excitation of higher order modes of an equilateral triangular dielectric resonator antenna," in *Proc. IEEE 7th Annu. Inf. Technol., Electron. Mobile Commun. Conf.*, Oct. 2016, pp. 1–4.

[32] S. A. Schelkunoff, *Electromagnetic Waves*. Princeton, NJ, USA: Van Nostrand, 1943, pp. 393–396.

[33] M. Abedian, H. Oraizi, S. K. A. Rahim, S. Danesh, M. R. Ramli, and M. H. Jamaluddin, "Wideband rectangular dielectric resonator antenna for low-profile applications," *IET Microw., Antennas Propag.*, vol. 12, no. 1, pp. 115–119, 2018.

[34] Z. N. Chen, N. Yang, Y.-X. Guo, and M. Y. W. Chia, "An investigation into measurement of handset antennas," *IEEE Trans. Instrum. Meas.*, vol. 54, no. 3, pp. 1100–1110, Jun. 2005.

[35] M. S. Iqbal and K. P. Esselle, "Pulse-preserving characteristics and effective isotropically radiated power spectra of a new ultrawideband dielectric resonator antenna," *IET Microw., Antennas Propag.*, vol. 12, no. 7, pp. 1231–1238, 2018.

[36] W.-W. Yang, W.-J. Sun, H. Tang, and J.-X. Chen, "Design of a circularly polarized dielectric resonator antenna with wide bandwidth and low axial ratio values," *IEEE Trans. Antennas Propag.*, vol. 67, no. 3, pp. 1963–1968, Mar. 2019.

ZHIWEI SONG was born in Tangshan, Hebei, China, in 1982. He received the B.S. degree in electronics information engineering and the M.S. degree in control theory and control engineering from the North China University of Science and Technology, Tangshan, in 2004 and 2013, respectively. He is currently pursuing the Ph.D. degree with the State Key Laboratory of Reliability and Intelligence of Electrical Equipment and the Key Laboratory of Electromagnetic Field and Electrical Apparatus Reliability of Hebei Province, School of Electrical Engineering, Hebei University of Technology, Tianjin, China. He engaged in antennas and computational electromagnetics, and currently involved on his Ph.D. thesis with the School of Electrical Engineering, on ultra-wide-band dielectric resonator antennas.

HONGXING ZHENG (M'01) received the Ph.D. degree in electronic engineering from Xidian University, Xi'an, in 2002.

He is currently a Professor with the School of Electronics and Information Engineering, Hebei University of Technology, Tianjin, China. He has authored six books and book chapters, and more than 200 journals and 100 conference papers. He holds 40 Chinese patents issued in 2018. His current research interests include wireless communication, design of microwave circuit and antenna, and computational electromagnetics. He is a Senior Member of the Chinese Institute of Electronics (CIE). He received the 2008 Young Scientists Award presented by the Tianjin Municipality, China, and was listed in the Who's Who in the World and Who's Who in the Science and Engineering in the World.

MENGJUN WANG was born in Baoding, Hebei, China, in 1978. He received the B.S. degree in information engineering and the M.S. degree in physical electronics from the Hebei University of Technology, Tianjin, China, in 1999 and 2005, respectively, and the Ph.D. degree from Tianjin University, Tianjin, in 2008. He is currently an Associate Professor with the School of Electronics and Information Engineering, Hebei University of Technology, Tianjin. His research interests include microwave radio-frequency technology, flexible electronics devices, and electromagnetic compatibility.

YAN LI was born in Gaomi, Shandong, China. She received the B.S. degree in electronic engineering from Changchun University, Changchun, China, in 2004, the M.S. degree in electronic engineering from Hebei University, Hebei, China, in 2011, and the Ph.D. degree from the Hebei University of Technology, in 2019. She is currently a Lecturer with the College of Information Engineering, China Jiliang University, Hangzhou, China. Her current research interests include signal integrity and power integrity, fast and efficient computational electromagnetics, electromagnetic modeling and experiment method, and its application in high-speed electronics.

TAO SONG was born in Dingzhou, Hebei, China. He received the B.S. degree in electronic science and technology and the M.S. degree in physical electronics from the Hebei University of Technology, Tianjin, China, in 2005 and 2008, respectively, where he is currently an Experimentalist with the Institute of Micro-Nano Photoelectron and Electromagnetic Technology Innovation.

His recent research interests include electromagnetic compatibility and near-field measurement.

ERPING LI (S'91–M'92–SM'01–F'08) received the Ph.D. degree in electrical engineering from Sheffield Hallam University, Sheffield, U.K., in 1992. From 1993 to 1999, he was a Senior Research Fellow, a Principal Research Engineer, an Associate Professor, and the Technical Director with the Singapore Research Institute and Industry. In 2000, he joined the Singapore National Research Institute of High Performance Computing, as a Principal Scientist, and the Director of the Department of the Electronics and Photonics. He is also a Distinguished Professor with Zhejiang University. He has authored or coauthored more than 400 articles in the referred international journals and conferences, and authored two books. His research interests include electrical modeling and design of micro/nano-scale integrated circuits, 3D electronic package integration, and nano-plasmonic technology.

YONGJIAN LI (M'10) was born in Hebei, China, in 1978. He received the B.E., M.E., and Ph.D. degrees from the Hebei University of Technology (HEBUT), China, in 2002, 2007, and 2011, respectively. From 2009 to 2011, he was a Research Assistant with the UTS, Australia. He visited Ottawa University, Canada, as a Visiting Scholar, from 2016 to 2017. He is currently the Deputy Director of the State Key Laboratory of Reliability and Intelligence of Electrical Equipment. He is also a Professor with the School of Electrical Engineering, HEBUT. His research interests include measurement magnetic properties, modeling of magnetic materials, and power electronics.

● ● ●